ADVANCED MATERIALS INTERFACES
www.advmatinterfaces.de

Ephrin Micropatterns Exogenously Modulate Cell Organization in Organoid-Derived Intestinal Epithelial Monolayers

Enara Larrañaga, Vanesa Fernández-Majada, Samuel Ojosnegros, Jordi Comelles, and Elena Martinez**

Eph-ephrin signaling acts as spatial cue to define the tissue boundaries, the axonal growth, or the organization of compartmentalized tissues in vertebrates. By the regulation of tension, adhesion, and repulsion, intermingling of cells expressing the membrane-tethered ligand and cells expressing the membrane-tethered receptor is prevented. Despite being surface-bound, most of the studies addressing Eph-ephrin interactions use soluble ligands, which lack the spatial component needed to study tissue patterning. Here, it is shown that spatial patterns of ephrin ligands can modulate the organization of the different compartments in organoid-derived intestinal epithelial monolayers. A modified version of the microcontact printing technique is used to create spatial cues of ephrin ligand on basement membrane surrogates. It is shown that both ligand concentration and cellular density can impact the strength of the repulsive effect triggered by Eph-ephrin signaling. Finally, it is demonstrated that by using micropatterned ephrin spatial cues one can modify the orientation of intestinal crypts and align them in the direction set by the pattern. The approach presented here is believed to be an excellent tool to study exogenous signal with relevant spatial distribution in vivo.

1. Introduction

Eph receptors constitute the largest group of transmembrane receptor tyrosine kinases. In vivo, they are involved as key regulators in the formation of tissue boundaries during development and the maintenance of tissue organization in adult organisms.[1–3] Eph receptors are classified as EphA and EphB receptors based on their sequence similarities and specificity for their ligands.[4] These ligands, the ephrins, are not soluble but tethered to the cell surface. Because both ligand and receptor are at the cell membrane, Eph-ephrin signaling occurs when cells are in contact with each other, and their binding leads to the clustering of both components, which has been shown as needed for activation.[5] Signaling can occur bidirectionally because ephrins themselves can transduce signals upon binding to Eph proteins. Signaling through the Eph receptors by ephrins is known as forward signaling and it is the canonical signaling pathway, while the opposite is known as reverse signaling.[6] This pathway involves the alteration of the actin cytoskeleton through the modulation of the main elements of the Rho GTPases family, resulting in the increase of actomyosin contractility and the inhibition of lamellipodia formation.[5,6]

Eph-ephrin signaling is essential to many aspects of tissue self-organization both during development and in adult organisms. It plays an important role during embryonic tissue boundary formation and the directional migration of developing axons. During mesoderm-ectoderm border formation, expression of ephrinB ligands and Eph receptors in both tissues leads to segregation through a process involving bi-directional forward signaling mediated by RhoA and Rac activity at the mesoderm/ectoderm boundary.[7] Eph-ephrin signaling is also involved in the formation of actomyosin cables that define the interface of the notochord-presomitic mesoderm border.[8] Similar Eph-ephrin-related actomyosin cables are found in the formation of hindbrain segment borders in early development.[9] Furthermore, Eph-mediated forward signaling regulation of actin dynamics via activation of the small Rho GTPases is involved in axon guidance by controlling collapse and retraction of the growth cone and retraction of neurites.[1,10]

Eph-ephrin signaling is also essential in maintaining the appropriate organization of the intestinal tissue in adult

E. Larrañaga, V. Fernández-Majada, J. Comelles, E. Martinez
Biomimetic Systems for Cell Engineering
Institute for Bioengineering of Catalonia (IBEC)
Carrer Baldiri i Reixac 15-21, Barcelona 08028, Spain
E-mail: jcomelles@ibecbarcelona.eu; emartinez@ibecbarcelona.eu

S. Ojosnegros
Bioengineering in Reproductive Health
Institute for Bioengineering of Catalonia (IBEC)
The Barcelona Institute of Science and Technology (BIST)
Carrer Baldiri i Reixac 4-8, Barcelona 08028, Spain

J. Comelles, E. Martinez
Department of Electronics and Biomedical Engineering
University of Barcelona (UB) Barcelona
Martí Franquès, 1, Barcelona 08028, Spain

E. Martinez
Biomedical Research Center - Bioengineering, Biomaterials and Nanomedicine
Monforte de Lemos 3-5., Pabellón 11. Planta 0, Madrid 28029, Spain

The ORCID identification number(s) for the author(s) of this article can be found under https://doi.org/10.1002/admi.202201301.

DOI: 10.1002/admi.202201301

organisms. Intestinal epithelia are composed by a heterogeneous cell population that includes enterocytes, transient amplifying cells, Paneth cells, and intestinal stem cells (ISCs), among others.[11–13] These different cell types are spatially segregated in vivo in differentiated villus (formed by enterocytes and secretory cells) and proliferative crypt regions (formed by transient amplifying cells, Paneth cells, and ISCs). This is achieved through a set of signaling gradients along the crypt-villus axis that establish the compartmentalization of the epithelium.[14] Among other signals, ephrinB1 concentration decreases from the tips of the villi to the base of the crypts, where the EphB2-expressing cells reside, contributing to the segregation of cell populations.[15,16] Newly generated absorptive enterocytes express EphB, but as they move up and away from the crypt, they shift to ephrinB expression. Eph-ephrin signaling prevents the intermingling of the differentiated and proliferating cells, leading to tissue compartmentalization. Its role is prominent in Paneth cells, which are differentiated cells retaining high levels of EphB, which prevent them from moving up. Therefore, they remain at the base of the crypts where they develop their secretory function. Remarkably, cell segregation onto villus-like and crypt-like regions has shown to be preserved on intestinal epithelial monolayers in vitro when employing organoid-derived cells.

While much of the original work on Eph-ephrin effects used soluble ligands,[17,18] using ligands tethered on surfaces could better mimic Eph-ephrin interactions, allowing the systematic study of Eph-ephrins as positional cues for tissue patterning. For instance, surface-bound ephrinB1 was used to show that integrin-mediated cell attachment was critically dependent on ephrin density.[19] Also, by using nanopatterned lipidic bilayers' substrates it has been demonstrated that ligand-receptor clustering is key in cell behavior and misregulation seems to be correlated with the invasive potential of breast cancer cells.[20,21] We recently showed that ephrin ligands nanopatterned onto substrates induced a strong receptor oligomerization, improving the cluster efficiency of conventional delivery systems using soluble ligands.[22] It should be noticed that all these experiments were dealing with single cell behavior onto nanoclustered ligands and, despite being undoubtedly useful to study the receptor–ligand interactions at the molecular level, do not address how ephrin (or Eph) patterns act as positional cues in tissue's organization. This last problem has been successfully addressed to study neuronal outgrowth by producing ephrin patterns at the microscale using printing approaches. In this regard, geometrically defined gradients of substrate-bound ephrinA5 were successfully used to study growth cone navigation in vitro.[23,24] Yet, other examples of ephrin patterns leading to tissue's organization in vitro are scarce.[23,25–28]

To address the role of ephrins as positional cues in tissue organization, patterning must be applied on proper cell-friendly and biomimetic substrates. In vivo, tissues sit on thin, dense forms of extracellular matrix (ECM) known as the basement membrane (BM), mainly composed of collagen type IV and laminin.[29] Patterning ephrins on BM surrogates such as laminin coatings or soft and sticky Matrigel is an unavoidable requirement to extend the application of ephrin patterns to complex tissues such as organoid-derived intestinal epithelia.[30] Here, we use the microcontact printing technique to create positional cues of clustered ephrinB1 ligands onto BM surrogates. We show that ephrinB1 patterns retain their biological activity and that the signaling strength can be effectively controlled by the micropatterns. Interestingly, our results indicate that despite high cell density tuning down the strength of ephrin spatial cues, surface-bound ephrinB1 can be used as an external cue to modulate the position, shape, and orientation of intestinal crypt-like structures on organoid-derived intestinal epithelial monolayers.

2. Results

2.1. Micropatterns of EphrinB1 Retain the Biological Activity of the Ligand

In previous works, we had established a protocol to anchor ephrinB1 ligands to glass surfaces coated with poly-L-lysine through the microcontact printing technique and we verified that the printed ligands were effective in stimulating the clustering and activation of EphB2 receptors in human epithelial kidney cells (HEK293T).[22,31] Based on this previous experience, we decided to study the effects of ephrinB1 forward signaling in the intestinal epithelium, where the ligand is differentially expressed and defines tissue organization.[9,16,32] However, cells such as those derived from intestinal organoids need to be cultured onto ECM-coated substrates. Thus, we first determined whether ephrinB1 micropatterns could be produced on top of laminin-coated surfaces through microcontact printing and if these ligands retained their biological activity after the printing procedure. And, to reduce the complexity of the system, for these first experiments we employed a cell line that endogenously express EphB2 receptors.

Figure 1a outlines the sequential steps for the microcontact printing technique of ephrinB1 ligands onto laminin-coated surfaces. The procedure involves the use of a polydimethylsiloxane (PDMS) stamp onto which the ephrinB1 molecules are adsorbed before being transferred to the substrate upon the conformal contact between the surface and the stamp. EphrinB1 ligands need to be dimerized to activate their membrane EphB2 receptors. Effective receptor activation requires the ephrinB1 ligands in solution to be presented in clusters, and the activation level is highly sensitive to ligand cluster size.[18,22] To produce such clusters, ephrinB1 ligands are commercialized as dimers fused to Fc groups and linked through disulfide bridges, named as ephrinB1/Fc ligands. These Fc groups are used to link dimers together by incubating them in a solution containing anti-Fc antibodies (Figure 1b). We had previously determined that upon 30 min of incubation with anti-Fc antibodies, mostly tetramers (dimers of ephrinB1/Fc dimers) of hydrodynamic diameters of ≈70 nm are obtained.[22] These clusters (referred to as ephrinB1 ligands) are the species that we employed to "ink" the PDMS stamps and are transferred to the surfaces. On the other hand, as controls, only Fc molecules clustered through anti-Fc antibodies are used (referred to as Fc molecules).

Micropatterns of ephrinB1 and Fc in the shape of 20 μm wide lines with a pitch of also 20 μm were then performed on top of the laminin-coated surfaces. To check for the success of the microcontact printing process, the micropatterns produced were visualized by immunofluorescence. It could be

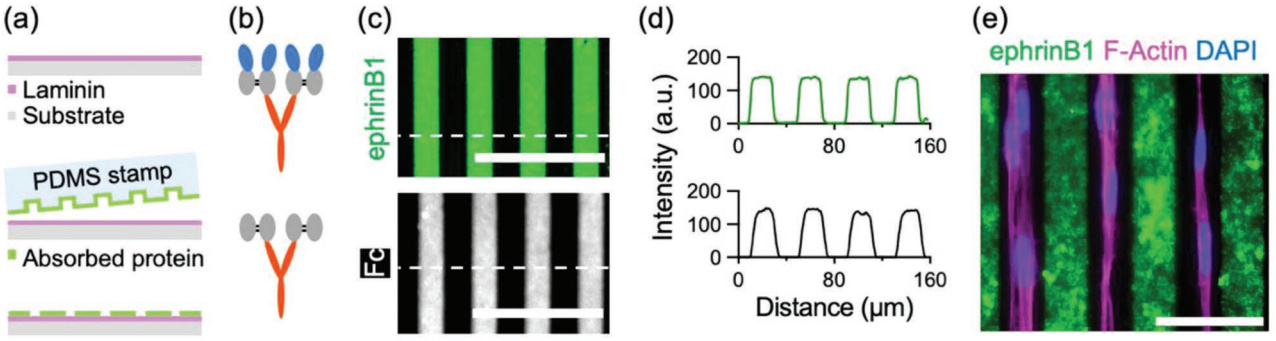

Figure 1. a) Scheme depicting the microcontact printing procedure followed to transfer ephrinB1 and Fc species onto laminin-coated substrates. First, the substrate was incubated with a laminin solution. Then, the microcontact printing procedure was performed on the surface. b) Schematic diagram showing the strategy to form clusters of ephrinB1 and Fc dimers (in blue and grey, respectively) through conjugation via anti-Fc antibodies (in red). c) Representative fluorescence microscopy images of micropatterns fabricated by microcontact printing. For visualization, ephrinB1 and Fc were immunostained. Scale bars: 100 μm. d) Fluorescence intensity profiles corresponding to the dash lines depicted in (c), showing the uniformity of the micropatterns for ephrinB1 (upper panel) and Fc (lower panel). The uniformity of the ephrinB1 lines was measured as Mean ± SD of maximum values: 138.1 ± 2.6 for ephrinB1 and 139.9 ± 5.3 for Fc. The edge definition was measured as Mean ± SD of distance between maximum and minimum: 1.8 ± 0.8 μm for ephrinB1 and 4.2 ± 0.6 μm for Fc. $N = 3$. e) Immunofluorescence image of ephrinB1 and NIH/3T3 cells stained for F-Actin and cell nuclei (DAPI). Scale bar: 100 μm.

then assessed that the printed lines had very good uniformity, high contrast, and edge definition (Figure 1c). The coverage of ephrinB1 and Fc species was investigated by plotting the fluorescence intensity of the images along the axis perpendicular to the lines (Figure 1d). For both micropatterns, there were abrupt changes in the fluorescence intensity that matched their dimensions with the theoretical width and separation of the lines (1.8 ± 0.8 μm edge for ephrinB1 and 4.2 ± 0.6 μm edge for Fc). Moreover, the structures printed were homogeneous with a variation of 2% in ephrinB1 signal and of 3% in Fc signal. Therefore, we could conclude that the microcontact printing technique employed was successful in creating micropatterns of ephinB1 and Fc onto laminin-coated substrates.

Once the patterns were produced, we wanted to check if the printed ligands retained their biological function and, in particular, if they were able to be recognized by EphB2 cell receptors. Upon ligand recognition, activated Eph receptors are known to act as positional cues in tissue patterning by regulating cell adhesion and repulsion.[33,34] It has been reported that cells expressing Eph receptors show strong morphological responses when exposed to linear micropatterns of ephrin ligands.[28] Here, we decided to present our ephrinB1 micropatterns to embryonic-derived fibroblasts (NIH/3T3), which express EphB2 receptors endogenously.[35] NIH/3T3 fibroblasts were cultured onto these micropatterns for 24 h. After this time, cells were fixed, immunostained for F-Actin, cell nuclei (4′,6-diamidino-2-phenylindole [DAPI]), and ephrinB1 (to localize the micropatterns), and imaged through fluorescence microscopy. Images showed that ephrinB1-EphB2 forward signaling was effective in inducing lamellipodia retraction, which resulted in cells occupying the ephrinB1-free regions (Figure 1e).

2.2. Cell Alignment Is Caused by EphrinB1-EphB2 Forward Signaling

At this point, we were wondering if these strong cell repulsive effects observed were due to EphB2-ephrinB1 forward signaling or were due to an increased affinity of the cells to adhere onto the laminin regions in between the ephrinB1 lines. To tackle this question, a set of experiments were performed seeding cells at a cell density of 10^5 cells cm^{-2} (cell surface density was low, so cells appeared as single entities) on micropatterns of 20 μm in size printed with ephrinB1 or with Fc species (**Figure 2**a). As controls, laminin-coated substrates were used. Cells on ephrinB1 patterns were confined between lines, while cells on Fc patterns could spread their lamellipodia in between and on Fc lines (Figure 2a). We could also observe that the main axis of the NIH/3T3 nucleus was oriented in the direction set by the ephrinB1 lines and that nuclei were rarely found on the patterned ephrinB1. To quantify these effects, we defined two quantities 1) a nucleus orientation index and 2) a nucleus position index. To obtain the first one, we ellipse fitted the nucleus and measured the angle (θ) between the ellipse main axis and the micropatterned lines (Figure 2b); the orientation index was then calculated as $\cos(2\cdot\theta)$ which is defined between −1 for nucleus perpendicular to the line ($\theta = 90°$) and 1 for nucleus parallel to the line ($\theta = 0°$). To obtain the nucleus position index we measured the fraction of area of the nucleus that was on a micropatterned line (Figure 2b), being 0 when there was no overlapping (nucleus between lines) and 1 when there was complete overlapping. As shown in Figure 2c, ephrinB1 strongly influenced cell nuclei orientation, which were aligned with the micropattern axis (orientation index ≈ 1), while Fc micropatterns and control substrates showed no preferred orientation (orientation index ≈ 0). Also, despite the presence of Fc lines per se producing some confinement of the cell nuclei (nuclei on top of the lines, in between lines, or without a preferred position), this effect was significantly enhanced when ephrinB1 was present on the laminin-coated substrates (Figure 2d). These results confirmed that ephrinB1 micropatterns trigger a cell repulsive effect and, therefore, the ligand retains its biological activity after the printing procedure and can induce ephrinB1-EphB2 forward signaling.

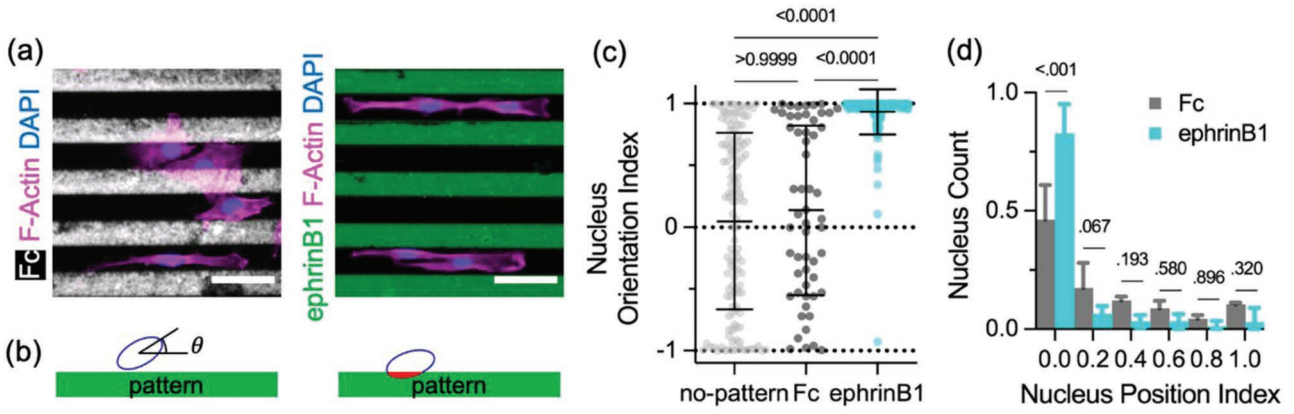

Figure 2. a) Representative fluorescence images of NIH/3T3 cells cultured at a cell seeding density of 10^5 cells cm^{-2} on micropatterns of Fc and ephrinB1 species (lines of 20 μm in size) produced on laminin-coated substrates. Images are immunostained for ephrinB1, Fc, F-Actin, and cell nuclei (DAPI). Scale bars: 100 μm. b) Schematic drawing showing the angle between the major axis of the fitted ellipse with respect of the pattern (θ), and the nucleus position with respect to the pattern, which is performed quantifying the red area showed in the scheme. c) Nucleus orientation index. Mean ± SD. *p*-values corresponding to a Kruskal–Wallis test. $N = 3$ experiments, $n = 3$ for no-pattern; $N = 2$ experiments, $n = 6$ for Fc; and $N = 9$ experiments, $n = 9$ for ephrinB1. d) Normalized histograms of the cell nuclei number as a function of the nucleus position index. Mean ± SD. *p*-values corresponding to a Tukey's test. $N = 2$ experiments, $n = 6$ for Fc; and $N = 9$ experiments, $n = 9$ for ephrinB1.

2.3. EphrinB1 Signaling Strength Can Be Effectively Controlled through Micropatterning

In vivo, cells of the crypts of the small intestine are subjected to complementary gradients of Eph-ephrin receptor–ligand signals, which indicates that ephrin signaling depends on their concentration.[15,16] Indeed, it has also been reported in experiments in vitro that ephrin might allow cell adhesion or trigger cell repulsion depending on the ligand concentration.[19,33,34] Therefore, once we knew that ephrinB1 micropatterns were biologically active, we investigated whether the strength of the EphB2-ephrinB1 forward signaling could be regulated by this technique. We fabricated a set of ephrinB1 micropatterns of lines of 20 μm in size on laminin-coated substrates where we varied the ephrinB1 concentration of the solutions used to "ink" the PDMS stamps. A broad range of ephrinB1 concentrations ranging from 1 to 10^{-4} dilutions from the stock concentration (69.0 μg mL^{-1} ephrinB1/Fc + 0.559 mg mL^{-1} anti-Fc antibodies) were tested. On the micropatterns produced, NIH/3T3 fibroblasts were seeded at a density of 10^5 cells cm^{-2} (low cell density leading to single cells) and cultured for 24 h. After this time, samples were fixed, immunostained for F-Actin, cell nuclei (DAPI), and ephrinB1, and imaged with a fluorescence microscope. Then, we quantified cell nuclei orientation with respect to the line direction, and cell nuclei position with respect to the patterns for the different ephrinB1 dilutions tested, as readouts of forward signaling.

We observed that the dilution of the ephrinB1 ligand produced micropatterns with gradients in ephrinB1 fluorescence intensities (**Figure 3**a and Figure S1a, Supporting Information). We could also visually assess that, when decreasing ephrinB1 concentration, its effects on directing cell orientation and position in between lines were progressively lost. This was quantitatively evaluated for the cell nuclei orientation, where we found a transition triggered by the ephrinB1 dilution (Figure 3b and Figure S1b, Supporting Information). For the highest ephrin concentrations, cells showed strongly elongated morphologies and were almost fully aligned parallel to the lines (orientation index ≈ 1). In addition, they were strongly confined in between the ephrinB1 lines (position index distribution centered at ≈0) (Figure 3c). When reducing the ephrin concentration, cells showed an increasingly spread morphology, a random orientation (orientation index ≈ 0), and a random distribution over all the cell culture area (position index homogeneously distributed). For the lowest dilution, ephrinB1 cell repulsive effects completely disappeared. Taking these results together, we can conclude that ephrinB1 ligands presented as micropatterns elicit a cellular response that can be modulated by changing the ligand concentration printed.

2.4. Cell Density Modulates the Effects of EphB2-EphrinB1 Forward Signaling

NIH/3T3 fibroblasts are mesenchymal cells and at a seeding concentration of 10^5 cells cm^{-2} are individualized on the surface. Bearing that in tissues such as intestinal epithelia, cells are densely packed, establishing cell–cell contacts, we decided to explore the effect of cell density on the strength of ephrinB1-EphB2 forward signaling. To do so, cell response was evaluated by screening for several cell seeding densities (10^5, 3×10^5, or 5×10^5 cells cm^{-2}) and two line widths (10 and 20 μm) (Figure S2, Supporting Information), and measured by the orientation and position of cell nuclei with respect to the micropatterned lines. Representative images showed that indeed NIH/3T3 fibroblasts' morphology, orientation, and position were strongly influenced by the presence of the ephrinB1 micropatterns with respect to the controls (**Figure 4**a). Moreover, when cultured at high density (5×10^5 cells cm^{-2}), cells on the ephrinB1 micropatterns formed packed cell clusters, in contrast to the more spread cell monolayers observed on non-patterned substrates. NIH/3T3 aggregates on 20 μm ephrinB1 lines were twice as packed as clusters on 10 μm lines and non-patterned controls

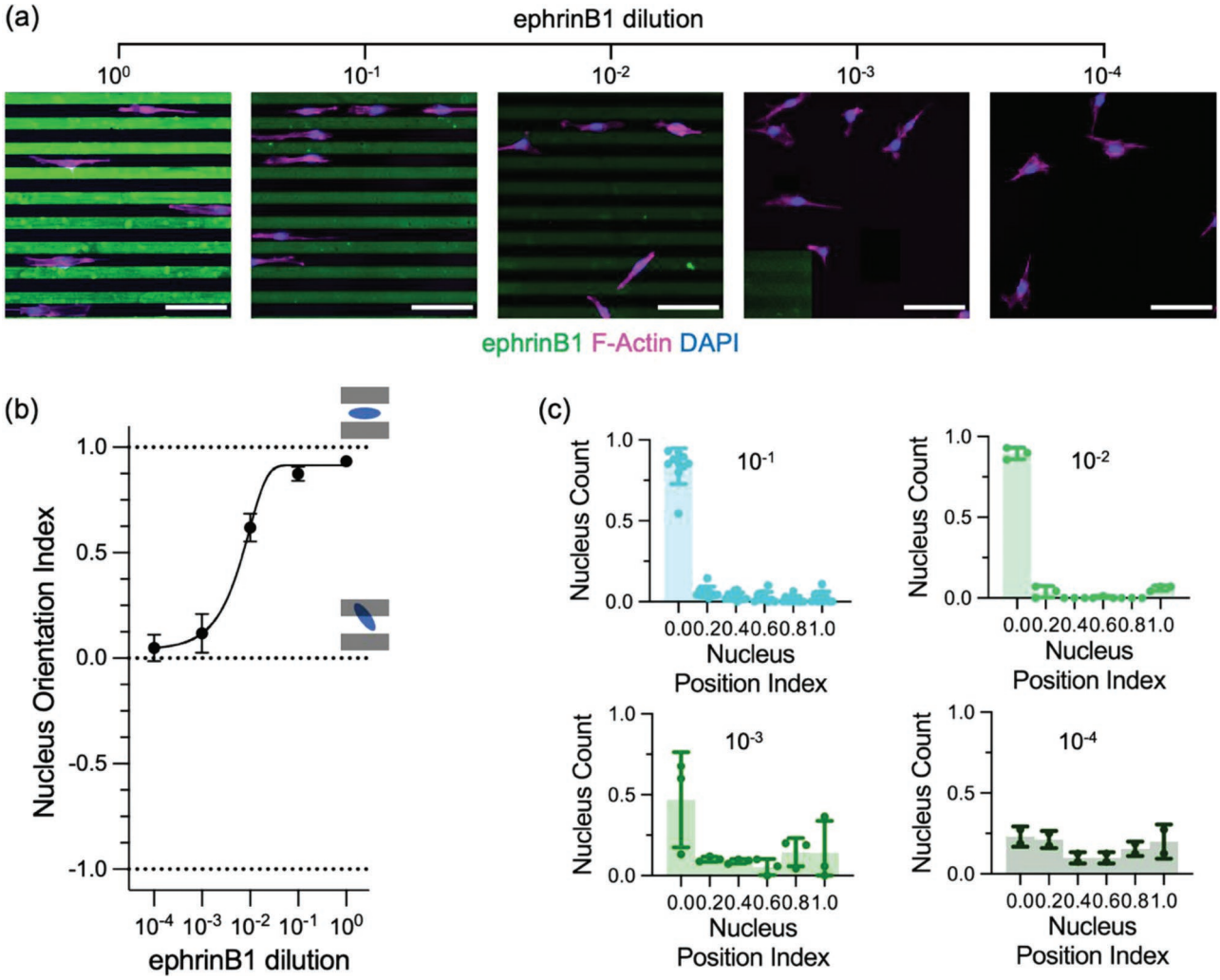

Figure 3. a) Representative fluorescence images for NIH/3T3 cells cultured on ephrinB1 micropatterns of lines of 20 µm in size printed on laminin-coated substrates. The micropatterns have been produced using ephrinB1 solutions at several dilutions. Images were generated upon immunostaining of ephrinB1, F-Actin, and cell nuclei (DAPI). Scale bars: 100 µm. b) Nucleus orientation index as a function of the ephrinB1 concentration. The symbols correspond to the experimental measurements, and the solid line is a fitting of the data using an allosteric modulator (logEC50). Data are plotted as mean ± SEM. $N \geq 3$ experiments. c) Normalized histograms of the cell nuclei number as a function of the nucleus position index for different ephrinB1 concentrations. Mean ± SD. $N \geq 3$ experiments.

(Figure S3, Supporting Information). In general, for all the cell seeding densities tested, cell nuclei were aligned with the micropattern axis (nucleus orientation index > 0.5) for both line sizes tested (Figure 4b). However, the highest degree of alignment was obtained for cells seeded at the lowest density of 10^5 cell cm^{-2} on the lines of 20 µm in width (orientation index ≈ 1). Then, the analysis of the nucleus position with respect to the pattern revealed that NIH/3T3 fibroblasts positioning strongly depended on the pattern size and the cell seeding density (Figure 4c). For lines of 10 µm in width, cell nuclei did not position preferentially with respect to the micropatterns (position index values were homogeneously distributed), probably because the line width was not large enough when compared to the nucleus size. On the other hand, at high cell seeding densities, cell nuclei were also not showing any preferential position with respect to the patterns, probably because cells established cell–cell contacts that were indeed dictating their location. For the lowest cell seeding density of 10^5 cells cm^{-2} and micropatterns of 20 µm width, almost all nuclei were fully positioned in between the ephrinB1 lines. Therefore, for the ephrinB1 concentration tested, by increasing the density of NIH/3T3 fibroblasts, EphB2-expressing cells are not excluded to spread on ephrinB1 regions but ephrinB1 micropatterns are still capable to orient packed cellular clusters in the direction imposed by the lines.

2.5. Microcontact-Printed EphrinB1 Induces Elongation and Alignment of Crypt-Like Structures on Organoid-Derived Intestinal Epithelial Monolayers

Finally, we addressed the effects of ephrinB1 forward signaling in primary intestinal epithelial cells obtained from mice

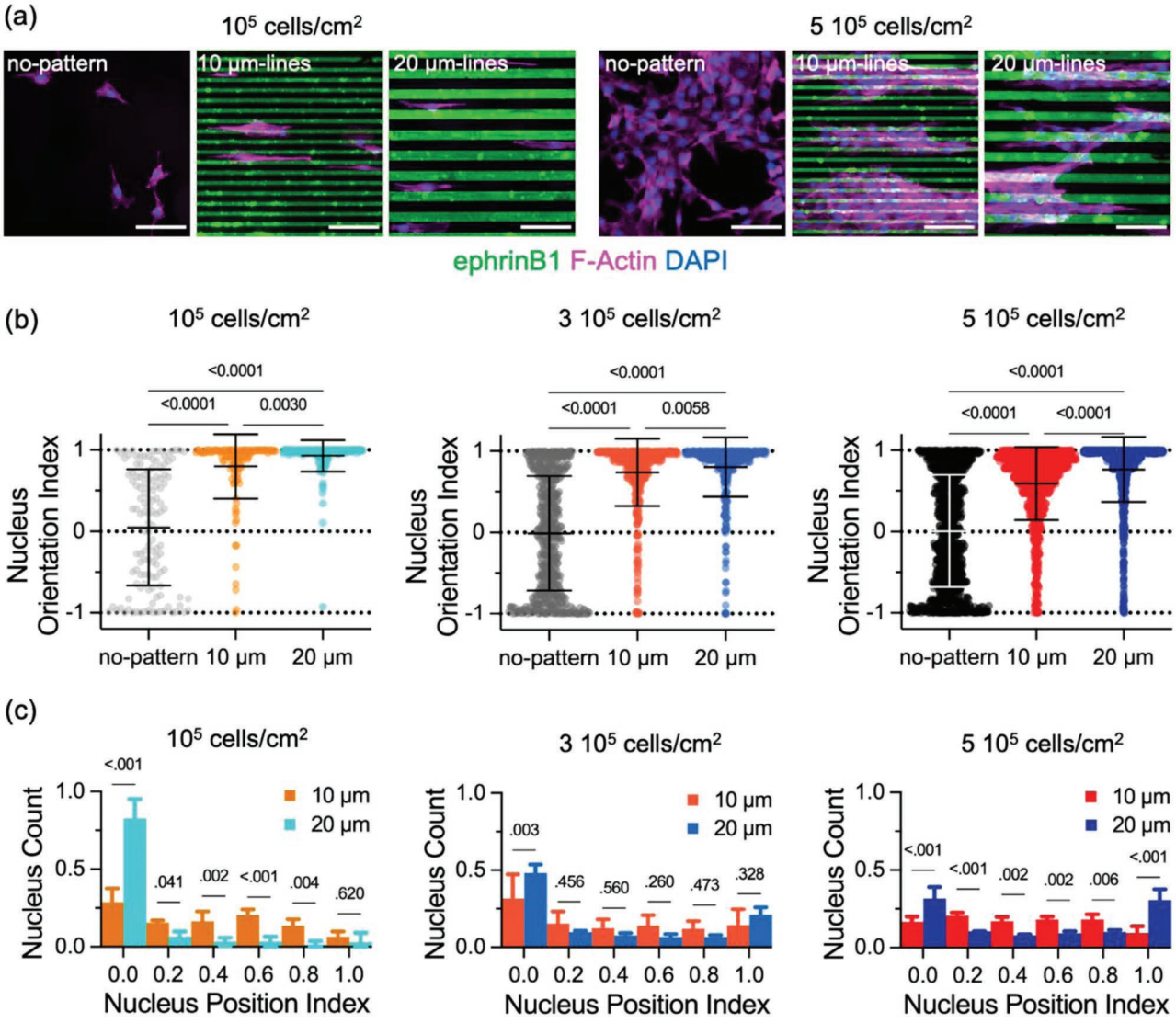

Figure 4. a) Representative fluorescence images of NIH/3T3 fibroblasts cultured onto ephrinB1 micropatterns produced on laminin-coated substrates. Images were obtained upon immunostaining of ephrinB1, F-Actin, and cell nuclei (DAPI). Experiments of two different cell densities and two pattern sizes are shown. As control, laminin substrates were employed. Scale bars: 100 µm. b) Nucleus orientation index for three different cell densities. Mean ± SD. *p*-values corresponding to a Kruskal–Wallis test. $N \geq 3$ experiments. c) Normalized histograms of the cell nuclei number as a function of the nucleus position index for three different cell densities. Mean ± SD. *p*-values corresponding to a Tukey's test. $N \geq 3$ experiments.

intestines and cultured in vitro as organoids. These organoid-derived cells can grow in vitro forming intestinal epithelial monolayers when cultured on a BM surrogate. This is commonly achieved by using collagen coatings, mixtures of collagen and laminin coatings, or Matrigel.[30,36,37] Here, we used a thin layer of Matrigel to coat cell culture substrates. Since stamping micropatterns on Matrigel while preserving its integrity is challenging, we used a technique involving freeze-drying that we had previously developed (**Figure 5**a).[38] In brief, cell culture substrates were coated by a thin layer of diluted Matrigel solution that was cross-linked at 37 °C for 1 h, then submerged in liquid N_2 and immediately brought to a low-pressure atmosphere to conduct the sublimation process. EphrinB1 micropatterns were then stamped on the freeze-dried Matrigel following the standard microcontact printing procedure. Finally, Matrigel coating was reconstituted by adding phosphate buffer saline (PBS) buffer. Immunofluorescence images showed that the ephrinB1 motifs were faithfully transferred to the Matrigel-coated surfaces while preserving the integrity of the underlying BM for a wide range of shapes and dimensions, as seen from laminin fluorescent signal and scanning electron microscopy images of the Matrigel (Figure 5b,c and Figure S4, Supporting Information). Then, single cells derived from intestinal epithelial organoids were seeded on the micropatterned Matrigel-coated surfaces. Cells formed a monolayer that was maintained in culture for 48 h. After this time, laminin coating was rearranged by the epithelial cells but ephrinB1 lines were still visible despite few inhomogeneities appeared (Figure 5d and Figure S5, Supporting Information). This showed that the non-even spatial

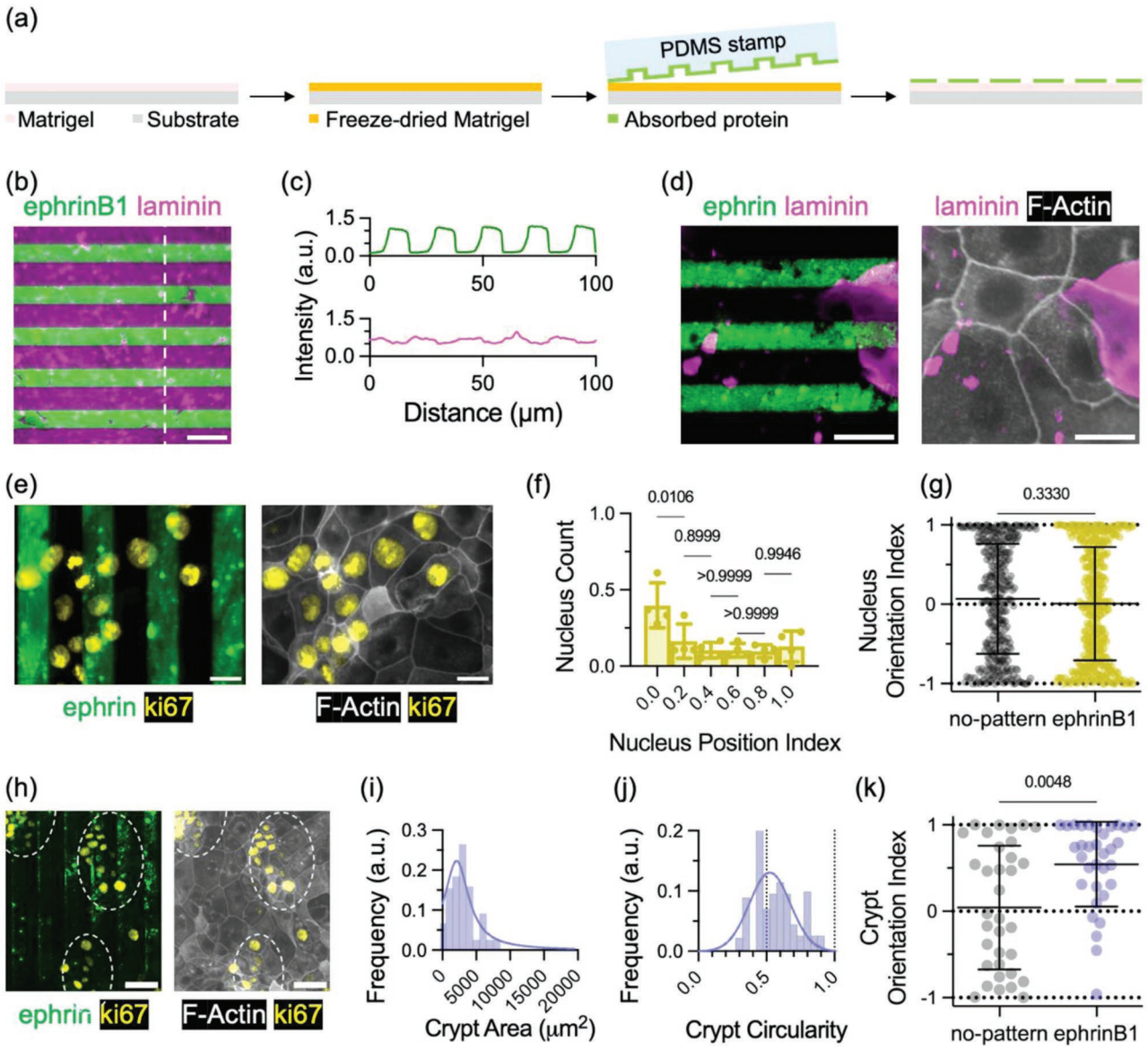

Figure 5. a) Scheme depicting the microcontact printing procedure to transfer biomolecules onto Matrigel-coated substrates. First, Matrigel-coated substrates were freeze-dried (Matrigel was diluted at 0.25 mg mL^{-1}). Then, the microcontact printing procedure was performed on the dried surfaces and afterward, samples were reconstituted with PBS. b) Representative fluorescence image of micropatterns of ephrinB1 ligands printed on treated Matrigel-coated substrates. Samples were immunostained for ephrinB1 and laminin. Scale bar: 20 μm. c) Fluorescence intensity profiles corresponding to the dashed line depicted in (b), showing the uniformity of the micropatterns for ephrinB1 (upper panel) and laminin (lower panel). d) Representative fluorescence images of IECs cultured onto ephrinB1 micropatterns produced on Matrigel-coated substrates. Images were obtained upon immunostaining of ephrinB1, laminin, and F-Actin. Scale bars: 20 μm. e) Representative fluorescence images of IECs cultured onto ephrinB1 micropatterns produced on Matrigel-coated substrates. Images were obtained upon immunostaining of ephrinB1, F-Actin, and proliferative cells (Ki67). Scale bars: 20 μm. f) Normalized histograms of the proliferative cell nuclei number as a function of the proliferative nucleus position index. Mean ± SD. *p*-values corresponding to a Kruskal–Wallis test. $N = 4$ experiments. g) Proliferative nucleus orientation index. Mean ± SD. *p*-values corresponding to a Mann–Whitney test. $N = 4$ experiments. h) Representative fluorescence images of IECs cultured onto ephrinB1 micropatterns produced on Matrigel-coated substrates. Images were obtained upon immunostaining of ephrinB1, F-Actin, and proliferative cells (Ki67). The white dashed line circles indicate proliferative crypt-like domains. Scale bars: 20 μm. i) Crypt area distribution. The bars correspond to the experimental measurements, and the solid line is the fitting of the data using a Gaussian function. $N = 3$ experiments. j) Crypt circularity distribution. The bars correspond to the experimental measurements, and the solid line is the fitting of the data using a Gaussian function. $N = 3$ experiments. k) Crypt orientation index. Mean ± SD. *p*-values corresponding to a Mann–Whitney test. $N = 3$ experiments.

distribution of ephrinB1 was still present at longer periods, thus potentially triggering EphB2-ephrinB1 forward signaling from the initial moment of cell adhesion to the late organization of the intestinal epithelia.

Organoid-derived intestinal epithelial cells form monolayers that might be locally packed, leading to high cell densities. Taking into account that we have shown that cell density may impact the strength of ephrinB1 micropattern signaling and the

10 μm lines produced a weak effect on cells, we selected 20 μm width lines to maximize the strength of the ephrinB1 forward signaling. We have previously demonstrated that these monolayers self-organize in proliferative and non-proliferative compartments. Proliferative regions are characterized by cells staining positive for the Ki67 proliferation marker and containing Lgr5+ stem cells (Figure S6a, Supporting Information) and Paneth cells (Figure S6b, Supporting Information), being analogous to crypt-like regions (Figure S6c, Supporting Information) surrounded by CK-20 positive differentiated cells (Figure S6d, Supporting Information).[30] So, we stained our monolayers for the Ki67 marker, which is a good label to localize crypt-like regions (Figure 5e) and observed that Ki67-positive cells did not align in the direction of the ephrinB1 lines (average value of the nucleus orientation index ≈ 0) (Figure 5g), but were preferentially located in the space between lines (higher frequency for nucleus position index close to ≈0) (Figure 5f). Therefore, we could see that despite the high cell density intrinsic to epithelia, ephrinB1 lines could efficiently modulate the position of proliferative crypts. Moreover, when looking at Ki67-positive cells as a collective (Figure 5h), we found that these aggregates (with typical sizes of ≈25 000 μm^2) (Figure 5i) were deviating from an isotropic circular shape. When ellipse-fitting the aggregates, we could observe that their circularity was close to ≈0.5 (Figure 5j), for both crypts on lines and non-patterned substrates (Figure S7, Supporting Information). This was corresponding to a more elongated ellipse-like shape that allowed us to obtain a main axis and its orientation vis-à-vis the direction of the ephrinB1 lines. We could observe that crypts on ephrinB1 lines were effectively biased in the direction of the lines (orientation index ≈ 0.75) (Figure 5k). Therefore, by using microcontact-printed ephrinB1 lines, we could modulate the orientation of Ki67-positive cell aggregates assimilated to the crypt-like domains of the organoid-derived intestinal epithelium.

3. Discussion

Eph-ephrin forward signaling is present in multiple tissues in vivo and it is a key signaling pathway to form and maintain tissue boundaries and organization from early development to adult organisms. Because both the receptor and the ligand are tethered to the cell membrane,[5] Eph-ephrin act as spatial cues that can direct axonal growth,[23] set the position of a tissue boundary,[9] or maintain tissue compartmentalization.[15,16] In the present work, we sought to validate surface-bound ephrin patterns as spatial cues to modulate cell behavior, specifically, the organization of organoid-derived intestinal epithelial monolayers. First, we showed that ephrin clusters could successfully be microcontact-printed on surrogates of the BM while retaining their biological function. Previous works have already shown that ephrin patterns can be transferred to BM surrogates such as laminin coatings,[19,23] here we extended it to more complex and physiology-like BM surrogates such as Matrigel coatings by adapting a technique that we previously developed.[38] By freeze-drying the Matrigel, we prevented the BM surrogate to get damaged during the stamping process, as we could assess by scanning electron microscope and laminin immunostaining. This may be partially related to the fact that Matrigel dilutions that generate homogenous coating prior the freeze-drying process were used.[38] Thus BM surfaces obtained after sublimation were more even, what may lead to a successful stamping. Noteworthy, laminin appeared rearranged after organoid-derived intestinal epithelial cells grew on ephrinB1 lines. Since ephrinB1 lines seemed fairly preserved, it is not clear if the differential distribution of laminin occurred by the rearrangement of the laminin in between ephrinB1 lines or by de novo secreted BM, which has been previously linked to ephrinB1 expression in cardiomyocytes.[39] Nonetheless, the ephrinB1 patterns were still visible showing that exogenous signaling was still active at longer time periods.

Microcontact-printed ephrin clusters prevented lamellipodia of EphB2-expressing fibroblasts to grow, resulting in cells elongating in the space between ephrin lines. Similar behavior was previously reported for retinal ganglion cells, that extended their axons guided by neighboring repulsive ephrinA5 lines.[25] Interestingly, we found out that the strength of ephrin-mediated "repulsion" was dependent on two factors: 1) the amount of ephrin stamped on the BM surrogate and 2) the cell density. In the first case, by changing the ephrin surface density we were able to efficiently modulate the alignment of fibroblasts in the space between lines. By progressively diluting the ephrin solution, EphB2-expressing fibroblasts were gradually able to grow lamellipodial structures on the ephrin lines which ultimately resulted in cells evenly spreading on the surface and losing the confinement and alignment observed when ephrin density was sufficiently high. This impact of ephrin surface density on the repulsive effects experienced by fibroblasts was evocative of the ability of retinal ganglion cells to discriminate between different protein concentrations of ephrinA5.[23] Also, epithelial-like and endothelial-like cells have been reported to showcase in vitro integrin activation depending on ephrinB1 surface density.[19] These cells displayed ephrinB1-induced attachment in a biphasic fashion when cultured on surfaces uniformly coated with ephrinB1 at different densities. Cell attachment through the activation of $\alpha_5\beta_1$ integrin in epithelial cells and $\alpha_V\beta_3$ integrin in endothelial cells increased when increasing ephrinB1 surface density until reaching a maximum, and gradually decreased for higher densities of ephrinB1. Due to the nature of the microcontact printing technique, it is difficult to estimate the actual ephrin density stamped on the BM surrogate, but our results are compatible with cell response in the second part of the biphasic curve.

More strikingly, the strength of the ephrinB1 repulsive effects was modulated by cell density. Despite mesenchymal cells such as NIH/3T3 do not form strong cell–cell contacts, they formed cell clusters that grew on top of the ephrin lines when the number of cells increased. Cells were individually aligned in the direction imposed by the lines, resulting in clusters of EphB2-expressing cells oriented by the surface-bound ephrinB1 pattern. It has been shown that EphB2-expressing cells increase homotypic contacts by a cadherin independent mechanism in the presence of ephrinB1.[40] This could explain why at high cell densities NIH/3T3 cells form packed cell aggregates that collectively spread over multiple ephrinB1 lines but orient in the direction of the lines as each individual cell is balancing the repulsion experienced by the ephrinB1 lines and

the increased adhesion to other EphB2-expressing cells. Similarly, when decreasing pattern size below the typical cell width, single cells start spreading on ephrinB1 lines but still align parallel to them.

Interestingly, when organoid-derived intestinal epithelial single cells were grown on ephrin patterns they behaved similarly. These organoid-derived cells contained two subpopulations: proliferative cells and Paneth cells with an increased expression of EphB2 receptor and differentiated cells with an increased expression of ephrinB1 ligand.[15,16] It has been shown that Eph signaling results in the regulation of cell intermingling: Eph-ephrin forward signaling raises interfacial tension and decreases cell contact through cortical actomyosin contractility between heterotypic cells, driving segregation by minimizing the overall interfacial tension both in vitro and in vivo.[40] In our experiments, the two cell populations segregated as well, resulting in the formation of proliferative clusters surrounded by differentiated cells.[30] These cell clusters, which are expected to be expressing EphB2-receptor were elongating and aligning in the direction of the ephrinB1 lines like NIH/3T3 EphB2-expressing fibroblasts when cultured at high cell density. Altogether, these results suggest that Eph-ephrin forward signaling triggered the clustering of EphB2-expressing cells. In the case of fibroblasts, they formed compact clusters contrary to the typical spread monolayer on non-patterned substrates, which suggests the minimization of the interfacial tension between cells and the substrate containing surface-bound ephrin lines. In the case of organoid-derived intestinal epithelial cells, signaling comes from the combination of the surface-bound ephrin and the membrane-tethered ephrin leading to 1) the appearance of compact proliferative clusters that 2) are oriented in the direction imposed by the ephrin lines.

4. Conclusions

Our results show that microcontact printing can be used to create biologically active ephrin spatial cues on different types of BM surrogates and that outcome of the signal will depend on the amount of surface-bound ephrin and the cell density. It was already reported that the strength of the signal could be modulated by controlling the density of the surface-bound ephrin in the context of axonal growth.[23] Now we showed that the strength of the ephrin signal can be also modulated by cell density and that it has an impact on the self-organization of organoid-derived intestinal epithelial monolayers. We believe that the work presented here has the potential to facilitate the study of exogenous signals which act as spatial cues in the native tissue.

5. Experimental Section

Preparation and Characterization of EphrinB1 Micropatterns on Hard and Soft Substrates: The masters fabricated by UV-photolithography and reactive ion etching (D+T Microelectrónica AIE) were silanized using a trichloro(1*H*,1*H*,2*H*,2*H*-perfluorooctyl)silane (Sigma-Aldrich) for 1 h in a vacuum chamber. The masters were silanized to avoid adhesion of the PDMS to their surface. PDMS replicas were freshly prepared mixing Sylgard 184 Silicon Elastomer and curing agent (Dow Corning) at a ratio of 10:1 w/w. PDMS was spun-coated onto the silicon masters and cured for 3 h at 65 °C. The design consisted of lines of equal width and pitch spacing (L = 10 or 20 µm). The stamps where incubated with 69 µg mL^{-1} recombinant mouse ephrinB1/Fc ligand (R&D Systems) or recombinant Human IgG1 Fc (R&D Systems) in a clustered fashion for 45 min at room temperature (RT). Clusters were prepared conjugating ligand (ephrinB1 fused to Fc, named ephrinB1/Fc) and control (only Fc) dimers with anti-Fc antibodies (Jackson ImmunoResearch) at 2:5 molar ratio for 30 min under constant shaking.[18,22]

Onto hard substrates such as laminin-coated substrates, the microcontact printing was applied directly.[19,23] The PDMS stamp was put in contact with the substrate, a 35 mm glass-bottom Petri dish (Mattek) functionalized with laminin (Invitrogen) at 20 µg mL^{-1} for 90 min at RT. However, onto soft hydrogels such as Matrigel, these were previously subjected to a freeze-drying process to make them mechanically resistant to sustain the PDMS stamp pressure, following a process developed by the research group.[38] In short, Ibidi plates were coated with Matrigel diluted at 0.25 mg mL^{-1} with DMEM/F-12 (Invitrogen). After gelation (1 h at 37 °C), the excess of the solution was removed, and samples were carefully rinsed first with PBS and then with Milli-Q water to avoid the presence of salts. Subsequently, samples were freeze-dried by immersion in liquid nitrogen and vacuum dried for 24 h at −50 °C and 0.06 mbar of pressure (1-4 LD-2, Christ Alpha). Microcontact printing was then carried out on the freeze-dried Matrigel. Finally, Matrigel substrates were reconstituted adding PBS at RT for at least 30 min at 37 °C.

The substrates were characterized by immunofluorescence. Substrates were blocked with a blocking buffer containing 1% BSA (Sigma-Aldrich) and 3% donkey serum (Millipore) in PBS for 30 min. Antibodies were diluted in PBS containing 0.1% BSA, and 0.3% donkey serum. The following antibodies were employed: as primary antibody anti-laminin (1:200, Abcam); as secondary antibodies, Alexa Fluor 488 goat anti-goat, and Alexa Fluor 647 donkey anti-rabbit (all from Jackson ImmunoResearch) diluted at 1:500. Finally, samples were mounted with Fluoromount (Thermo Fisher). Fluorescence images were acquired using an epifluorescence inverted microscope (Axio Observer 7, Carl Zeiss) with 63× oil objective (NA = 1.4). Images were acquired at randomly selected locations.

The Matrigel-coated substrates were also characterized by using a scanning electron microscopy (NOVA NanoSEM 230 microscope, FEI). The diluted Matrigel were freeze-dried and placed on an aluminum sample dish fixed with a conductive silver paint for optimal imaging. The following parameters were used: 4 spot size, 87.5 Pa chamber pressure, 6.0 mm working distance, and 5 kV accelerating high voltage.

The ephrin lines were characterized by quantifying their uniformity and their edge definition. To define both uniformity and edge definition, fluorescence images showing the micropatterns were employed. To this procedure, the intensity profile was generated from the fluorescence intensity values encompassed along a line perpendicular to the micropatterns. Next, the uniformity was calculated as the mean value of the intensity and the edge definition was the difference between the minimum and maximum value of the intensity.

Cell Culture: NIH/3T3 mouse embryonic fibroblasts (ATCC CRL-1658) were maintained at 37 °C in a humidified incubator under a 5% CO_2 atmosphere in DMEM (Gibco) medium supplemented with 10% fetal bovine serum (Life Technologies), 1% L-glutamine (Gibco), 1% sodium pyruvate (Invitrogen), and 1% penicillin–streptomycin (Sigma-Aldrich). For the experiments, cells were trypsinized and cultured for 24 h at densities of 10^5, 3×10^5, or 5×10^5 cell cm^{-2}. These cell densities were selected to obtain single cells or cells connecting with each other.

Intestinal epithelial cells (IECs) were obtained through mechanical and enzymatical digestion of full-grown intestinal organoids isolated from *Lgr5-EGFP-IRES-creERT2* mice.[30] These organoid-derived single cells were cultured with advanced DMEM/F12 (Invitrogen) medium supplemented with 1% Glutamax (Gibco), 1% HEPES (Sigma-Aldrich), Normocin (1:500, Invitrogen), 2% B27 (Gibco), 1% N_2 (Gibco), and 1.25 mM N-acetylcysteine (Sigma-Aldrich) plus recombinant murine EGF (100 ng mL^{-1}, Gibco), recombinant murine Noggin (100 ng mL^{-1},

Peprotech), recombinant human R-spondin 1 (200 ng mL^{-1}, R&D Biosystems), CHIR99021 (3 µM), valproic acid (1 mM), and ROCK inhibitor Y-27632 (10 µM, Sigma-Aldrich). For the experiments, cells were seeded at a density of 10^5 cells and cultured for 48 h to obtain a confluent monolayer. The medium was changed at 24 h.

Cells were fixed with 10% neutralized formalin (Sigma-Aldrich) for 40 min at 4 °C, permeabilized with 0.5% Triton X-100 (Sigma-Aldrich) for 30 min at RT, and blocked for at least 2 h at RT with a blocking buffer containing 1% BSA (Sigma-Aldrich), 3% donkey serum (Millipore), and 0.2% Triton X-100 in PBS. All primary antibodies were diluted in 0.1% BSA, 0.3% donkey serum, and 0.2% Triton X-100 in PBS and incubated on cells overnight at 4 °C. Primary antibodies used were: anti-Ki67 (1:100, Abcam) and anti-laminin (1:200, Abcam). Secondary antibodies were diluted in 0.1% BSA and 0.3% donkey serum in PBS and incubated on cells 1 h at RT. Alexa Fluor 488 donkey anti-goat, Alexa Fluor 647 donkey anti-goat, and Alexa Fluor 647 donkey anti-rabbit (all from Jackson ImmunoResearch) were diluted at 1:500. Alexa Fluor 568 phalloidin was used to stain filamentous actin (F-Actin). Nuclei were stained with DAPI (1:1000). Finally, samples were mounted with Fluoromount (Thermo Fisher). Fluorescence images were acquired using an epifluorescence inverted microscope (Axio Observer 7, Carl Zeiss) with 10× air (NA = 0.30), 20× air (NA = 0.40) objectives, and 63× oil objective (NA = 1.4). Images were acquired at randomly selected locations.

Orientation and Position with Respect to Biochemical Patterns: To define the orientation and position of cell nuclei or crypt-like domains with respect to the linear patterns, fluorescence images showing both the cells and the micropatterns were employed. To this procedure, the images of cell nuclei were segmented from the DAPI or Ki67 intensity channels and subjected to a median filter with a radius of 1 µm to remove the noise, homogenize the staining, and prevent losing the edges. The crypt-like domains were segmented from the Ki67 intensity channel and subjected to a mean filter with a radius of 3 µm. The protein patterning images were subjected to a mean filter with a radius of 2 µm to smoothen stamp edges. Next, the filtered images were segmented using the default ImageJ threshold function to obtain binary masks. To remove the background noise, the binary masks were eroded twice and dilated twice. After threshold, fused nuclei were separated, performing a watershed segmentation. Finally, single objects touching the edges of the image were removed. To obtain the orientation index, cell nuclei were ellipse fitted using ImageJ to extract their major and minor axis. Then, the orientation index was calculated as cos (2θ), where θ was the angle between the major axis of the nucleus and the patterned lines, and had a value between –1 and 1 by definition. The nucleus position with respect to the lines was quantified using ImageJ as well. Using the redirect tool of this program, the fraction of the nucleus area overlapping with the micropatterns (Area $\text{nucelus}_{\text{on pattern}}$/Area $\text{nucleus}_{\text{Total}}$) was computed. A nucleus completely overlapping the micropattern had position index equal to 1, a nucleus that does not overlap a patterned area had a nucleus position index equal to 0, and a nucleus partially overlapping a micropatterns had a nucleus position index between 0 and 1. Analogously for the crypts, the same equations were used, but using the whole crypt-like domain instead of the nucleus.

Statistical Analysis: Statistical analysis was done using GraphPad Prism software (GraphPad Software Inc.). Results were presented as mean ± standard deviation or as mean ± standard error of the mean. The number of experiments from which data were extracted was specified in each case. Normality of the datasets was tested by the d'Agostino–Pearson normality test. The tests used to assess for statistical differences are specified in the figure caption as well as the *p*-value obtained.

Supporting Information

Supporting Information is available from the Wiley Online Library or from the author.

Acknowledgements

Funding for this project was provided by European Union Horizon 2020 (ERC grant no. 647863 – COMIET and 2020 FET-Open grant no. 828931 – BRIGHTER), Spanish Ministry of Science and Innovation, and Severo Ochoa Program for Centres of Excellence in R&D in Spain (2016–2019). The results presented here only reflect the views of the authors; the European Commission is not responsible for any use that may be made of the information it contains.

Conflict of Interest

The authors declare no conflict of interest.

Data Availability Statement

The data that support the findings of this study are available from the corresponding author upon reasonable request.

Keywords

eph-ephrin, microcontact printing, organoid-derived intestinal epithelia, tissue organization

Received: June 12, 2022
Revised: August 2, 2022
Published online:

[1] J. Egea, R. Klein, *Trends Cell Biol.* **2007**, *17*, 230.
[2] J. Cayuso, Q. Xu, D. G. Wilkinson, *Dev. Biol.* **2015**, *401*, 122.
[3] H. Taylor, J. Campbell, C. D. Nobes, *Curr. Biol.* **2017**, *27*, R90.
[4] E. N. Committee, *Cell* **1997**, *90*, 403.
[5] R. Klein, *Development* **2012**, *139*, 4105.
[6] E. B. Pasquale, *Cell* **2008**, *133*, 38.
[7] N. Rohani, L. Canty, O. Luu, F. Fagotto, R. Winklbauer, *PLoS Biol.* **2011**, *9*, e1000597.
[8] F. Fagotto, N. Rohani, A. S. Touret, R. Li, *Dev. Cell* **2013**, *27*, 72.
[9] S. Calzolari, J. Terriente, C. Pujades, *EMBO J.* **2014**, *33*, 686.
[10] J. Huot, *Prog. Neuro-Psychopharmacol. Biol. Psychiatry* **2004**, *28*, 813.
[11] M. Bjerknes, H. Cheng, *Methods Enzymol.* **2006**, *419*, 337.
[12] N. Barker, J. H. van Es, J. Kuipers, P. Kujala, M. van den Born, M. Cozijnsen, A. Haegebarth, J. Korving, H. Begthel, P. J. Peters, H. Clevers, *Nature* **2007**, *449*, 1003.
[13] T. Sato, J. H. Van Es, H. J. Snippert, D. E. Stange, R. G. Vries, M. Van Den Born, N. Barker, N. F. Shroyer, M. Van De Wetering, H. Clevers, *Nature* **2011**, *469*, 415.
[14] L. Meran, A. Baulies, V. S. W. Li, *Stem Cells Int.* **2017**, *2017*, 7970385.
[15] J. Holmberg, M. Genander, M. M. Halford, C. Annere, M. Sondell, M. J. Chumley, R. E. Silvany, M. Henkemeyer, J. Frisén, *Cell* **2006**, *125*, 1151.
[16] E. Batlle, J. T. Henderson, H. Beghtel, M. M. W. Van den Born, E. Sancho, G. Huls, J. Meeldijk, J. Robertson, M. Van de Wetering, T. Pawson, H. Clevers, *Cell* **2002**, *111*, 251.
[17] M. P. Beckmann, D. P. Cerretti, P. Baum, T. V. Bos, L. James, T. Farrah, C. Kozlosky, T. Hollingsworth, H. Shilling, E. Maraskovsky, F. A. Fletcher, V. Lhotak, T. Pawson, S. D. Lyman, *EMBO J.* **1994**, *13*, 3757.
[18] E. Stein, A. A. Lane, D. P. Cerretti, H. O. Schoecklmann, A. D. Schroff, R. L. Van Etten, T. O. Daniel, *Genes Dev.* **1998**, *12*, 667.

[19] U. Huynh-Do, *EMBO J.* **1999**, *18*, 2165.
[20] K. Salaita, P. P. M. Nair, R. R. S. Petit, R. R. M. Neve, D. Das, J. W. Gray, J. T. Groves, *Science* **2010**, *327*, 1380.
[21] T. Lohmüller, Q. Xu, J. T. Groves, *Nano Lett.* **2013**, *13*, 3059.
[22] V. Hortigüela, E. Larrañaga, F. Cutrale, A. Seriola, M. García-Díaz, A. Lagunas, J. Andilla, P. Loza-Alvarez, J. Samitier, S. Ojosnegros, E. Martínez, *Nano Lett.* **2018**, *18*, 629.
[23] A. C. von Philipsborn, S. Lang, J. Loeschinger, A. Bernard, C. David, D. Lehnert, F. Bonhoeffer, M. Bastmeyer, *Development* **2006**, *133*, 2487.
[24] S. Lang, A. C. Von Philipsborn, A. Bernard, F. Bonhoeffer, M. Bastmeyer, *Anal. Bioanal. Chem.* **2008**, *390*, 809.
[25] F. Brinkmann, M. Hirtz, A. M. Greiner, M. Weschenfelder, B. Waterkotte, M. Bastmeyer, H. Fuchs, *Small* **2013**, *9*, 3265.
[26] F. Fiederling, M. Weschenfelder, M. Fritz, A. Von Philipsborn, M. Bastmeyer, F. Weth, *eLife* **2017**, *6*, e25533.
[27] K. Truong, B. Leigh, J. T. Vecchi, R. Bartholomew, L. Xu, C. A. Guymon, M. R. Hansen, *Hear. Res.* **2021**, *409*, 108315.
[28] B. W. Tuft, L. Xu, B. Leigh, D. Lee, C. A. Guymon, M. R. Hansen, *J. Tissue Eng. Regener. Med.* **2018**, *12*, e1392.
[29] D. R. Sherwood, *Curr. Opin. Cell Biol.* **2021**, *72*, 19.
[30] G. Altay, E. Larrañaga, S. Tosi, F. M. Barriga, E. Batlle, V. Fernández-Majada, E. Martínez, *Sci. Rep.* **2019**, *9*, 10140.
[31] F. Cutrale, D. Rodriguez, V. Hortigüela, C. L. Chiu, J. Otterstrom, S. Mieruszynski, A. Seriola, E. Larrañaga, A. Raya, M. Lakadamyali, S. E. Fraser, E. Martinez, S. Ojosnegros, *Nat. Protoc.* **2019**, *14*, 616.
[32] M. A. Stimamiglio, E. Jiménez, S. D. Silva-Barbosa, D. Alfaro, J. J. García-Ceca, J. J. Muñoz, T. Cejalvo, W. Savino, A. Zapata, *J. Leukocyte Biol.* **2010**, *88*, 483.
[33] L. L. Kiessling, J. E. Gestwicki, L. E. Strong, *Angew. Chem., Int. Ed.* **2006**, *45*, 2348.
[34] P. W. Janes, E. Nievergall, M. Lackmann, *Semin. Cell Dev. Biol.* **2012**, *23*, 43.
[35] M. Zimmer, A. Palmer, J. Köhler, R. Klein, *Nat. Cell Biol.* **2003**, *5*, 869.
[36] C. A. Thorne, I. W. Chen, L. E. Sanman, M. H. Cobb, L. F. Wu, S. J. Altschuler, *Dev. Cell* **2018**, *44*, 624.
[37] C. Pérez-González, G. Ceada, F. Greco, M. Matejcic, M. Gómez-González, N. Castro, A. Menendez, S. Kale, D. Krndija, A. G. Clark, V. R. Gannavarapu, A. Álvarez-Varela, P. Roca-Cusachs, E. Batlle, D. M. Vignjevic, M. Arroyo, X. Trepat, *Nat. Cell Biol.* **2021**, *23*, 745.
[38] A. G. Castaño, V. Hortigïela, A. Lagunas, C. Cortina, J. Samitier, *RSC Adv.* **2014**, *4*, 29120.
[39] G. Genet, C. Guilbeau-Frugier, B. Honton, E. Dague, M. D. Schneider, C. Coatrieux, D. Calise, C. Cardin, C. Nieto, B. Payré, C. Dubroca, P. Marck, C. Heymes, A. Dubrac, D. Arvanitis, F. Despas, M. F. Altié, M. H. Seguelas, M. B. Delisle, A. Davy, J. M. Sénard, A. Pathak, C. Galés, *Circ. Res.* **2012**, *110*, 688.
[40] A. A. Kindberg, V. Srivastava, J. M. Muncie, V. M. Weaver, Z. J. Gartner, *J. Cell Biol.* **2021**, *220*, e202005216.